Estimation of the Velocity of a Walking Person in Non-Stationary Indoor Environments from the Received RF Signal

Rym Hicheri
Faculty of Engineering and Science
University of Agder
NO-4898 Grimstad, Norway
rym.hicheri@uia.no

Matthias Pätzold
Faculty of Engineering and Science
University of Agder
NO-4898 Grimstad, Norway
matthias.paetzold@uia.no

Néji Youssef
Ecole Supérieure des Communications de Tunis
Université de Carthage
2083 El Ghazala, Tunisia
neji.youssef@supcom.rnu.tn

***Abstract*—Accurate estimation of the time-variant (TV) velocity, i.e., TV speed and TV direction of motion, of walking persons in indoor environment is of great importance in a variety of wireless indoor applications. This paper presents a novel method for estimating the velocity of a walking person in three-dimensional indoor environments, which are assumed to be equipped with a distributed 3×3 multiple-input multiple-output (MIMO) system. The approach estimates the TV speed, TV vertical angle-of-motion (VAOM), and TV horizontal angle-of-motion (HAOM) by fitting the spectrogram of the complex channel gain of a non-stationary indoor channel model to the spectrogram obtained from the received radio signals. The validity of the estimation algorithm has been confirmed by comparing the estimated parameters of interest with their corresponding exact values, known from generated test signals.**

I. Introduction

The precise estimation of the time-variant (TV) velocity of moving objects/persons plays a key role in enabling a variety of mobile radio communications and indoor wireless applications.

In the context of mobile radio communications, precise estimation of the mobile stations' speed is required for the design of hand-off, adaptive modulation, and power control algorithms [1]. The developed estimators can be classified according to the statistical property they employ: level-crossings, covariance, maximum likelihood, and power spectrum. Crossing-based methods calculate the number of level-crossings of the envelope and/or phase of the received signal, which is proportional to the speed of the mobile station [2], [3]. Covariance-based approaches determine the speed of the mobile units by means of the maximum Doppler frequency information which can be extracted from the covariance of the received signal [4], [5]. It should be noted that crossing- and covariance-based estimation techniques require the a priori knowledge of the statistical properties of the fading channel. Due to the limited studies on non-stationary channel statistics, the applicability of these methods is limited to wide-sense stationary (WSS) channels. Maximum likelihood-based speed estimation techniques require the knowledge of the signal-to-noise ratio and are complex to implement [6], [7]. Power spectrum-based methods have been developed based on the differentiation and derivation of the power spectrum of the fading channel [8]–[10]. Although these approaches have been extended to non-isotropic scattering [10], their applicability is limited to WSS channels, for which the speed is assumed to be constant. Additionally, the aforementioned speed estimation procedures do not provide any information regarding the direction of motion of the mobile units.

In recent years, much attention has been paid to velocity-based human in-home activity tracking because of its key role in various wireless indoor applications, such as remote medical care, healthcare services, security and surveillance, and human-machine interaction [11]–[13]. Context-aware and wearable velocity-based devices can be classified according to the technique they are employing: video (image processing), sensor, and radio frequency (RF). Video-based in-home monitoring estimates the motion profile of moving/fixed objects/persons over time using a camera by detecting their boundaries [14]–[16]. Sensor-based human activity tracking in indoor environments can take the form of on-body or off-body devices which are equipped with sensors such as accelerometers, gyroscopes, and global positioning systems [17]–[20]. The RF-based motion tracking approach exploits the effects of a moving object/person on a received RF signal. The usefulness of this technique has been demonstrated by the Emerald [21], the mmVital [22], and the WiGait [23] devices. Interest in radar-based in-home activity tracking has also been growing due to its proven technology and safety [24]. As pointed out in [22], [25], and [24], RF-based approaches face several challenges, including their sensitivity to the rich scattering structure of indoor environments, i.e., fixed scatterers resulting from walls and furniture, and the TV direction of motion of the moving users.

Our objective is to contribute to the topic of indoor human activity monitoring by proposing a new iterative procedure to estimate the TV velocity of a single moving person in a three-dimensional indoor environment that considers the effects of both fixed and moving objects. For simplicity, the walking person is represented by a single moving scatterer that may represent any part of the person's body, e.g., the center of gravity, head or shoulder. The fixed scatterers represent the fixed objects in the room, such as walls, furniture, and decoration items. Here, the room is assumed to be equipped with a distributed 3×3 multiple-input multiple-output (MIMO) system. In the present work, the TV speed, TV vertical

 DOI: 10.1109/LATINCOM.2018.8613224

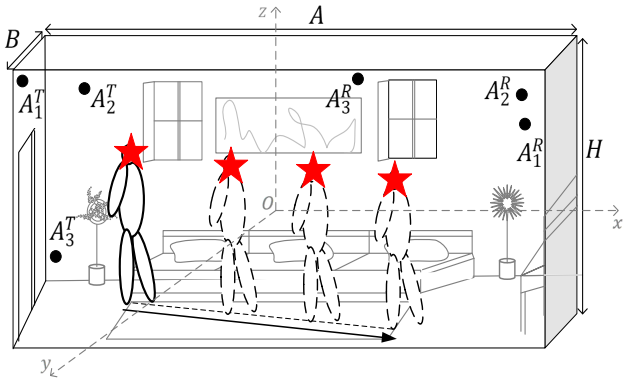

Fig. 1. Typical room architecture with distributed antennas, fixed objects (e.g., walls, furniture) and a walking person.

angle-of-motion (VAOM), and TV horizontal angle-of-motion (HAOM) are optimized by fitting the spectrograms of the model in [26] to the spectrograms of the received signals. Although the primarily objective of the proposed algorithm is to estimate the TV velocity, this task requires the determination of all channel parameters, i.e., gains, phases, TV azimuth (elevation) angles-of-departure (AAODs (EAODs)), and TV azimuth (elevation) angles-of-arrival (AAOAs (EAOAs)). The estimation of these parameters is based on the minimization of the Euclidean norm of the fitting error. Exact closed-form expressions have been derived for the estimates of the path gains corresponding to the moving scatterer (person) as well as the overall fixed scatterers. The validation of the introduced velocity estimation method is performed by comparing the estimated TV speed, TV VAOM, and TV HAOM with the corresponding true quantities. This task requires the prior knowledge of the speed and the direction of motion of the walking person. Unfortunately, this information cannot be obtained from measurement data. Therefore, the accuracy of the proposed procedure has been verified by comparing the obtained estimated parameters of interest with those of known test signals, generated by means of computer simulations.

The reminder of this paper is organized as follows. Section II presents some useful background material. The proposed estimation procedure is described in Section III. Numerical examples are provided in Section IV. Finally, the conclusion is drawn in Section V.

II. Background Material

A. Problem Description

The objective of this paper is to propose an accurate procedure to estimate the TV velocity, i.e., TV speed, TV VAOM, and TV HAOM, of a moving person in a three-dimensional indoor environment by exploiting the effects of the person's motion on the Doppler characteristics of the propagation medium. An example of a room architecture with six distributed antennas and a single moving person (★) is depicted in Fig. 1. Here, the scenario consists of a room with length A, width B, and height H centered at the origin O and equipped with a distributed 3×3 MIMO system consisting of three transmit antennas (A_1^T, A_2^T, and A_3^T) and

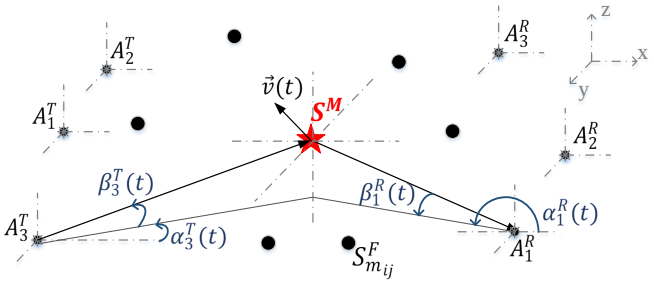

Fig. 2. Multipath propagation in the 3×3 MIMO indoor channel.

three receive antennas (A_1^R, A_2^R, and A_3^R). The propagation phenomenon taking place in the indoor area is modelled using the three-dimensional indoor multipath propagation scenario introduced in [26]. A simplified geometrical description of the propagation scenario is illustrated in Fig. 2. The fixed antennas A_1^T, A_2^T, A_3^T, A_1^R, A_2^R, and A_3^R are located at the positions (x_1^T, y_1^T, z_1^T), (x_2^T, y_2^T, z_2^T), (x_3^T, y_3^T, z_3^T), (x_1^R, y_1^R, z_1^R), (x_2^R, y_2^R, z_2^R), and (x_3^R, y_3^R, z_3^R), respectively. Moreover, it is assumed that there is only one person moving in the room, who is modelled by a single moving scatterer S^M (★). This person is located at the initial position (x^M, y^M, z^M) and moving with a TV velocity $\vec{v}(t)$. The trajectory of the moving point scatterer S^M is described by its TV speed $v(t) = |\vec{v}(t)|$, the TV VAOM $\beta_v(t)$, and the TV HAOM $\alpha_v(t)$. The TV positions $x(t)$, $y(t)$, and $z(t)$ along the x-, y- and z-axis of the moving person S^M can be deduced from the velocity $\vec{v}(t)$ according to [26, Eqs. (5)−(7)]. The fixed objects, seen between the jth transmit antenna A_j^T and the ith receive antenna A_i^R, are modelled by M_{ij} fixed scatterers $S_{m_{ij}}^F$ (•) $(m = 1, 2, ..., M_{ij})$. Furthermore, single-bounce scattering is assumed.

B. Spectrogram

Under the assumption of perfect channel state information (CSI) at the receiver side, the complex channel gain $\mu_{ij}(t)$ between the jth transmit antenna and ith receive antenna $(i, j = 1, 2, 3)$ can be expressed as [26]

$$\mu_{ij}(t) = c_{ij} \exp\left[j\theta_{ij}(t)\right] + \sum_{m_{ij}=1}^{M_{ij}} c_{m_{ij}} \exp\left(j\theta_{m_{ij}}\right). \quad (1)$$

Here, the first term refers to the component associated with the moving scatterer S^M, and the second term describes the multipath propagation component resulting from the M_{ij} fixed scatterers. Also, the quantities c_{ij} and $c_{m_{ij}}$ denote the gains of the moving scatterer and m_{ij}th fixed scatterer, respectively. The phases $\theta_{m_{ij}}$ are assumed to be independent and identically distributed random variables which are uniformly distributed over the interval $(0, 2\pi]$. In (1), the TV phase $\theta_{ij}(t)$ is expressed, in terms of the TV Doppler frequency $f_{ij}(t)$ caused by the motion of S^M and the initial phase of the channel $\theta_{ij,0}$, as $\theta_{ij}(t) = 2\pi \int_0^t f_{ij}(u)du + \theta_{ij,0}$, with

$$\begin{aligned} f_{ij}(t) = -f_{\max}(t) \big\{ &\cos(\beta_v(t)) \left[\cos(\beta_j^T(t)) \cos(\alpha_j^T(t) - \alpha_v(t)) \right. \\ &\left. + \cos(\beta_i^R(t)) \cos(\alpha_i^R(t) - \alpha_v(t))\right] + \sin(\beta_v(t)) \left[\sin(\beta_i^R(t)) \right. \\ &\left. + \sin(\beta_j^T(t))\right] \big\} \end{aligned} \quad (2)$$

where $f_{\max}(t) = f_0 v(t)/c_0$ is the TV maximum Doppler frequency, in which f_0 and c_0 denote the carrier frequency and the speed of light, respectively. In (2), $\beta_j^T(t)$ ($\beta_i^T(t)$) and $\alpha_j^T(t)$ ($\alpha_i^T(t)$) stand for the EAOD (EAOA) and AAOD (AAOA) corresponding to the jth transmit (ith receive) antenna, respectively. The TV angles $\beta_j^T(t)$, $\alpha_j^T(t)$, $\beta_i^R(t)$, and $\alpha_i^R(t)$ are expressed in terms of the TV positions of S^M and the positions of the transmit and receive antennas according to [26, Eqs. (10)−(13)]. Our main goal in this paper is to estimate the TV velocity $\vec{v}(t)$ of the moving person, represented by S^M, while taking into account the overall effect of the fixed scatterers regardless of the contribution of each fixed scatterer $S_{m_{ij}}^F$. In the following, the overall effect of the fixed scatterers will be described using a single complex term $C_{F_{ij}} \exp(j\vartheta_{F_{ij}})$, where $C_{F_{ij}} = \sqrt{(\sum_{m_{ij}=1}^{M_{ij}} c_{m_{ij}} \cos(\theta_{m_{ij}}))^2 + (\sum_{m_{ij}=1}^{M_{ij}} c_{m_{ij}} \sin(\theta_{m_{ij}}))^2}$ and $\vartheta_{F_{ij}} = \text{atan2}(\sum_{m_{ij}=1}^{M_{ij}} c_{m_{ij}} \sin(\theta_{m_{ij}}), \sum_{m_{ij}=1}^{M_{ij}} c_{m_{ij}} \cos(\theta_{m_{ij}}))$. According to [26], by approximating the Doppler frequencies $f_{ij}(t)$ by N piecewise linear functions, the spectrogram $S_{ij}(f,t)$ of $\mu_{ij}(t)$ can be expressed as

$$S_{ij}(f,t) = S_{ij}^{(a)}(f,t) + S_{ij}^{(c)}(f,t) \tag{3}$$

where $S_{ij}^{(a)}(f,t)$ and $S_{ij}^{(c)}(f,t)$ are called the auto-term and the cross-term of the spectrogram, respectively. The auto-term $S_{ij}^{(a)}(f,t)$ is given by

$$S_{ij}^{(a)}(f,t) = c_{ij}^2 G\big(f, f_{ij}(t), \sigma_{ij,1}^2\big) + G\bigg(f, 0, \frac{\sigma_0^2}{2}\bigg) C_{F_{ij}}^2 \tag{4}$$

in which $G(a,b,c) = \exp[-(a-b)^2/(2c)]/(\sqrt{2\pi c})$, $\sigma_0^2 = 1/(2\pi\sigma_w)^2$, and $\sigma_{ij,1}^2 = (\sigma_0^2 + \sigma_w^2 k_{ij}^2(t_l))/2$, with $k_{ij}(t_l)$ being defined according to [26, Eq. (25)] and σ_w^2 being the spread of the Gaussian window used for the computation of the spectrogram. After some mathematical manipulations, it can be shown that the cross-term $S_{ij}^{(c)}(f,t)$ in [26, Eq. (40)] can be written as

$$S_{ij}^{(c)}(f,t) = \frac{2c_{ij}C_{F_{ij}}}{\sigma_w\sqrt{\pi}} \Re\big\{ g_{ij}(t) G\big(f, m_{ij}(t), \sigma_{ij,3}^2\big) \cdot \exp\big(j\,(\theta_{ij}(t) - \vartheta_{F_{ij}})\big)\big\} \tag{5}$$

where $g_{ij}(t) = G(f_{ij}(t), 0, \sigma_{ij,2}^2 + \sigma_0^2)$, $m_{ij}(t) = \sigma_0^2 f_{ij}(t)/(\sigma_{ij,2}^2 + \sigma_0^2)$, and $\sigma_{ij,3}^2 = \sigma_{ij,2}^2\sigma_0^2/(\sigma_{ij,2}^2 + \sigma_0^2)$, in which $\sigma_{ij,2}^2 = \sigma_0^2 - jk_{ij}/(2\pi)$.

It should be noted that in practice the complex channel gain of the received signal is computed from samples of the channel at discrete time instances $t_p = p\Delta t \in [0,T]$, $p = 1,\ldots,P$, where T is the observation time interval and Δt refers to the time sampling period. Then, the spectrogram of the received signal is computed from samples with discrete frequencies $f_q = q\Delta f \in [-B/2, B/2]$, $q = 1,\ldots,Q$ and time instances t_p, where B and Δf are the frequency bandwidth and the frequency sampling period, respectively.

III. Estimation of the Time-Variant Velocity

This section deals with estimating the TV velocity of a moving person in an indoor environment, where the channel is modelled as described in Section II. Let $\hat{\mu}_{ij,p}$ denote the complex channel gain of a measured channel, and $\hat{S}_{ij}(f_q,t_p)$ the corresponding spectrogram. Here, the problem at hand is to determine, at each time instant t_p, a set of parameters $\mathcal{P}_p = \{\tilde{c}_{ij}, \tilde{k}_{ij,p}, \tilde{\theta}_{ij,0}, \tilde{C}_{F_{ij}}, \tilde{\vartheta}_{F_{ij}}, \tilde{v}_{ij,p}, \tilde{\alpha}_{j,p}^T, \tilde{\beta}_{j,p}^T, \tilde{\alpha}_{i,p}^R, \tilde{\beta}_{i,p}^R, \tilde{\alpha}_{v,p}, \tilde{\beta}_{v,p}\}$ in such a way that the spectrogram $\tilde{S}_{ij}(f_q,t_p)$ of the channel model in [26] matches $\hat{S}_{ij}(f_q,t_p)$. For this purpose, we introduce the objective function for determining $\mathcal{P}_p$ as

$$E(\mathcal{P}_p) = \left\| \begin{array}{c} \hat{S}_{11}(f_q,t_p) - \tilde{S}_{11}(f_q,t_p) \\ \hat{S}_{12}(f_q,t_p) - \tilde{S}_{12}(f_q,t_p) \\ \hat{S}_{13}(f_q,t_p) - \tilde{S}_{13}(f_q,t_p) \\ \hat{S}_{21}(f_q,t_p) - \tilde{S}_{21}(f_q,t_p) \\ \hat{S}_{22}(f_q,t_p) - \tilde{S}_{22}(f_q,t_p) \\ \hat{S}_{23}(f_q,t_p) - \tilde{S}_{23}(f_q,t_p) \\ \hat{S}_{31}(f_q,t_p) - \tilde{S}_{31}(f_q,t_p) \\ \hat{S}_{32}(f_q,t_p) - \tilde{S}_{32}(f_q,t_p) \\ \hat{S}_{33}(f_q,t_p) - \tilde{S}_{33}(f_q,t_p) \end{array} \right\|_2^2 . \tag{6}$$

The objective function in (6) is equivalent to that in (7) [see the top of the next page], where $\hat{\mathbf{S}}_{ij,p}$ and $\mathbf{G}$ are column vectors containing the stacked values of $\hat{S}_{ij}(f_q,t_p)$ and $G(f_q,0,\sigma_0^2/2)$ for increasing values of q, respectively. In (7), the quantities $\tilde{c}_{ij}$, $\tilde{C}_{F_{ij}}$, $\tilde{\theta}_{ij,0}$ and $\tilde{\vartheta}_{F_{ij}}$ denote the estimated values of c_{ij}, $C_{F_{ij}}$, $\theta_{ij,0}$ and $\vartheta_{F_{ij}}$, respectively. Also, the estimated TV Doppler frequencies $\tilde{f}_{ij,p}$ are expressed as $\tilde{f}_{ij,p} = -f_0\tilde{v}_p\{\cos(\tilde{\beta}_{v,p})[\cos(\tilde{\beta}_{j,p}^T)\cos(\tilde{\alpha}_{j,p}^T - \tilde{\alpha}_{v,p}) + \cos(\tilde{\beta}_{i,p}^R)\cos(\tilde{\alpha}_{i,p}^R - \tilde{\alpha}_{v,p})] + \sin(\tilde{\beta}_{v,p})[\sin(\tilde{\beta}_{i,p}^R) + \sin(\tilde{\beta}_{j,p}^T)]\}/c_0$, in which $\tilde{v}_p$, $\tilde{\beta}_{v,p}$, $\tilde{\alpha}_{v,p}$, $\tilde{\beta}_{j,p}^T$, $\tilde{\alpha}_{j,p}^T$, $\tilde{\beta}_{i,p}^R$, and $\tilde{\alpha}_{i,p}^R$ are the estimated values of $v(t_p)$, $\beta_v(t_p)$, $\alpha_v(t_p)$, $\beta_j^T(t_p)$, $\alpha_j^T(t_p)$, $\beta_i^R(t_p)$, and $\alpha_i^R(t_p)$, respectively. The instantaneous channel phase can be obtained as $\tilde{\theta}_{ij,p} = 2\pi\int_0^{t_p}\tilde{f}_{ij}(u)\,du + \tilde{\theta}_{ij,0}$. In (7), $\tilde{\sigma}_{ij,1,p}^2 = (\sigma_0^2 + \sigma_w^2\tilde{k}_{ij,p}^2)/2$, $\tilde{\sigma}_{ij,2,p}^2 = \sigma_0^2 - j\tilde{k}_{ij,p}/(2\pi)$, and $\tilde{\sigma}_{ij,3,p}^2 = \sigma_0^2\tilde{\sigma}_{ij,2,p}^2/(\tilde{\sigma}_{ij,2,p}^2 + \sigma_0^2)$, with $\tilde{k}_{ij,p}$ being the estimated value of $k_{ij}(t_p)$. For arbitrary chosen initial values of $\tilde{c}_{ij}^{(0)}$, $\tilde{k}_{ij,p}^{(0)}$, $\tilde{\theta}_{ij,0}^{(0)}$, $\tilde{C}_{F_{ij}}^{(0)}$, $\tilde{\vartheta}_{F_{ij}}^{(0)}$, $\tilde{v}_p^{(0)}$, $\tilde{\beta}_{v,p}^{(0)}$, $\tilde{\alpha}_{v,p}^{(0)}$, $(\tilde{\beta}_{j,p}^T)^{(0)}$, $(\tilde{\alpha}_{j,p}^T)^{(0)}$, $(\tilde{\beta}_{i,p}^R)^{(0)}$, and $(\tilde{\alpha}_{i,p}^R)^{(0)}$, the new estimates of $\tilde{c}_{ij}^{(l+1)}$, $\tilde{k}_{ij,p}^{(l+1)}$, $\tilde{\theta}_{ij,0}^{(l+1)}$, $\tilde{C}_{F_{ij}}^{(l+1)}$, $\tilde{\vartheta}_{F_{ij}}^{(l+1)}$, $\tilde{v}_p^{(l+1)}$, $\tilde{\beta}_{v,p}^{(l+1)}$, $\tilde{\alpha}_{v,p}^{(l+1)}$, $(\tilde{\beta}_{j,p}^T)^{(l+1)}$, $(\tilde{\alpha}_{j,p}^T)^{(l+1)}$, $(\tilde{\beta}_{i,p}^R)^{(l+1)}$, and $(\tilde{\alpha}_{i,p}^R)^{(l+1)}$ at every iteration l, $l = 0,1,...$, are obtained according to (8) [see the top of the next page]. For fixed values of $\tilde{c}_{ij}^{(l)}$, $\tilde{k}_{ij,p}^{(l)}$, $\tilde{\theta}_{ij,0}^{(l)}$, $\tilde{C}_{F_{ij}}^{(l)}$, $\tilde{\vartheta}_{F_{ij}}^{(l)}$, $\tilde{v}_p^{(l)}$, $\tilde{\beta}_{v,p}^{(l)}$, $\tilde{\alpha}_{v,p}^{(l)}$, $(\tilde{\beta}_{j,p}^T)^{(l)}$, $(\tilde{\alpha}_{j,p}^T)^{(l)}$, $(\tilde{\beta}_{i,p}^R)^{(l)}$, and $(\tilde{\alpha}_{i,p}^R)^{(l)}$, one can derive the right-hand side of (8) with respect to the variable $\tilde{c}_{ij}$, which shows that (8) reaches a minimum if the new estimate $x = \tilde{c}_{ij}^{(l+1)}$ satisfies the following cubic equation

$$2x^3\left\|\mathbf{y}_{ij}^{(l)}\right\|_2^2 + 3x^2\left(\mathbf{y}_{ij}^{(l)}\right)^T\mathbf{f}_{ij}^{(l)} + x\left[\left\|\mathbf{f}_{ij}^{(l)}\right\|_2^2 - 2\left(\hat{\mathbf{S}}_{ij,p}^{(l)} - \mathbf{G}\left(\tilde{C}_{F_{ij}}^{(l)}\right)^2\right)^T\mathbf{y}_{ij}^{(l)}\right] - \left(\mathbf{f}_{ij}^{(l)}\right)^T\left(\hat{\mathbf{S}}_{ij,p}^{(l)} - \mathbf{G}\left(\tilde{C}_{F_{ij}}^{(l)}\right)^2\right) = 0 \tag{9}$$

where $(\cdot)^T$ is the transpose operator. The column vectors $\mathbf{f}_{ij}^{(l)}$ and $\mathbf{y}_{ij}^{(l)}$ contain the stacked values of the functions $2\tilde{C}_{F_{ij}}^{(l)}/$

$$E(\mathcal{P}_p)=\sum_{i,j=1}^{3}\left\|\hat{\mathbf{S}}_{ij,p}-\tilde{c}_{ij}^2 G\Big(f_q,\tilde{f}_{ij,p},\tilde{\sigma}_{ij,1,p}^2\Big)-\mathbf{G}\tilde{C}_{F_{ij}}^2-\frac{2\tilde{c}_{ij}\tilde{C}_{F_{ij}}}{\sigma_w\sqrt{\pi}}\Re\Big\{\tilde{g}_{ij,p}G\big(f,\tilde{m}_{ij,p},\sigma_{ij,3,p}^2\big)\exp\Big(j\Big(\tilde{\theta}_{ij,p}-\tilde{\vartheta}_{F_{ij}}\Big)\Big)\Big\}\right\|_2^2 \quad (7)$$

$$\Big(\tilde{c}_{ij}^{(l+1)},\tilde{k}_{ij,p}^{(l+1)},\tilde{\theta}_{ij,0},\tilde{C}_{F_{ij}}^{(l+1)},\tilde{\vartheta}_{F_{ij}}^{(l+1)},\tilde{v}_p^{(l+1)},\tilde{\beta}_{v,p}^{(l+1)},\tilde{\alpha}_{v,p}^{(l+1)},(\tilde{\beta}_{j,p}^{T})^{(l+1)},(\tilde{\alpha}_{j,p}^{T})^{(l+1)},(\tilde{\beta}_{i,p}^{R})^{(l+1)},(\tilde{\alpha}_{i,p}^{R})^{(l+1)}\Big)=$$
$$\underset{\mathcal{P}_p}{\operatorname{argmin}}\left\{\sum_{i,j=1}^{3}\left\|\hat{\mathbf{S}}_{ij,p}-\tilde{c}_{ij}^2 G\Big(f_q,\tilde{f}_{ij,p},\tilde{\sigma}_{ij,1,p}^2\Big)-\mathbf{G}\tilde{C}_{F_{ij}}^2-\frac{2\tilde{c}_{ij}\tilde{C}_{F_{ij}}}{\sigma_w\sqrt{\pi}}\Re\Big\{\tilde{g}_{ij,p}G\big(f,\tilde{m}_{ij,p},\sigma_{ij,3,p}^2\big)\exp\Big(j\Big(\tilde{\theta}_{ij,p}-\tilde{\vartheta}_{F_{ij}}\Big)\Big)\Big\}\right\|_2^2\right\} \quad (8)$$

$$\Delta_0=108\left\|\mathbf{y}_{ij}^{(l)}\right\|_2^2\left[2\left(\hat{\mathbf{S}}_{ij,p}-\mathbf{G}\left(\tilde{C}_{F_{ij}}^{(l)}\right)^2\right)^T\mathbf{y}_{ij}^{(l)}-\left\|\mathbf{f}_{ij}^{(l)}\right\|_2^2\right]\left\|\mathbf{f}_{ij}^{(l)}\right\|_2^2\left(\mathbf{y}_{ij}^{(l)}\right)^T\left(\hat{\mathbf{S}}_{ij,p}-\mathbf{G}\left(\tilde{C}_{F_{ij}}^{(l)}\right)^2\right)+108\left(\left(\mathbf{y}_{ij}^{(l)}\right)^T\mathbf{f}_{ij}^{(l)}\right)^3\left(\mathbf{f}_{ij}^{(l)}\right)^T$$
$$\left(\hat{\mathbf{S}}_{ij,p}^{(l)}-\mathbf{G}\left(\tilde{C}_{F_{ij}}^{(l)}\right)^2\right)+9\left(\left(\mathbf{y}_{ij}^{(l)}\right)^T\mathbf{f}_{ij}^{(l)}\left[\left\|\mathbf{f}_{ij}^{(l)}\right\|_2^2-2\left(\hat{\mathbf{S}}_{ij,p}^{(l)}-\mathbf{G}\left(\tilde{C}_{F_{ij}}^{(l)}\right)^2\right)^T\mathbf{y}_{ij}^{(l)}\right]\right)^2-8\left\|\mathbf{y}_{ij}^{(l)}\right\|_2^2\left[\left\|\mathbf{f}_{ij}^{(l)}\right\|_2^2-2\left(\hat{\mathbf{S}}_{ij,p}^{(l)}-\mathbf{G}\left(\tilde{C}_{F_{ij}}^{(l)}\right)^2\right)^T\mathbf{y}_{ij}^{(l)}\right]^3$$
$$-108\left\|\mathbf{y}_{ij}^{(l)}\right\|_2^4\left(\left(\mathbf{f}_{ij}^{(l)}\right)^T\left(\hat{\mathbf{S}}_{ij,p}^{(l)}-\mathbf{G}\left(\tilde{C}_{F_{ij}}^{(l)}\right)^2\right)\right)^2 \quad (10)$$

$(\sigma_w\sqrt{\pi})\Re\{\tilde{g}_{ij,p}^{(l)}G(f,\tilde{m}_{ij,p}^{(l)},(\sigma_{ij,3,p}^{(l)})^2)\exp(j(\tilde{\theta}_{ij,p}^{(l)}-\tilde{\vartheta}_{F_{ij}}^{(l)}))\}$ and $G(f_q,\tilde{f}_{ij,p}^{(l)},(\tilde{\sigma}_{ij,1,p}^{(l)})^2)$ for increasing values of q, respectively. Since the cubic equation in (9) has real-valued coefficients, at least one of its roots x_k, $k=1,2,3$, is real. The roots x_k of (9) can be expressed as $x_k=-(b_0+\zeta^k A_0+B_0/(\zeta^k A_0))/(3a_0)$, where $\zeta=0.5(j\sqrt{3}-1)$, $a_0=2||\mathbf{y}_{ij}^{(l)}||_2^2$, $b_0=3(\mathbf{y}_{ij}^{(l)})^T\mathbf{f}_{ij}^{(l)}$, $B_0=b_0^2-3a_0[(||\mathbf{f}_{ij}^{(l)}||^2-2(\hat{\mathbf{S}}_{ij,p}-\mathbf{G}(\tilde{C}_{F_{ij}}^{(l)})^2)^T\ \mathbf{y}_{ij}^{(l)}]$, and $A_0=[(C_0\pm\sqrt{-27\Delta_0 a_0^2})/2]^{1/3}$, in which $C_0=2b_0^2-9a_0b_0[(||\mathbf{f}_{ij}^{(l)}||^2-2(\hat{\mathbf{S}}_{ij,p}-\mathbf{G}(\tilde{C}_{F_{ij}}^{(l)})^T\mathbf{y}_{ij}^{(l)}]-27a_0^2(\mathbf{f}_{ij}^{(l)})^T(\hat{\mathbf{S}}_{ij,p}^{(l)}-\mathbf{G}(\tilde{C}_{F_{ij}}^{(l)})$, and the discriminant Δ_0 is given in (10). Then, the new estimate of the gain $\tilde{c}_{ij}^{(l+1)}$ of the moving scatterer S^M corresponds to the real-valued root x_k that minimizes the right-hand side of (8). Similarly, it can be shown that (8) is minimized if the new estimate $x=\tilde{C}_{F_{ij}}^{(l+1)}$ satisfies

$$3x^2\mathbf{G}^T\mathbf{k}_{ij}^{(l)}+x\left[\left\|\mathbf{k}_{ij}^{(l)}\right\|^2-2\left(\hat{\mathbf{S}}_{ij,p}-\left(\tilde{c}_{ij}^{(l+1)}\right)^2\mathbf{y}_{ij}^{(l)}\right)^T\mathbf{G}\right]$$
$$+2x^3||\mathbf{G}||^2-\left(\mathbf{k}_{ij}^{(l)}\right)^T\left(\hat{\mathbf{S}}_{ij,p}-\left(\tilde{c}_{ij}^{(l+1)}\right)^2\mathbf{y}_{ij}^{(l)}\right)=0 \quad (11)$$

in which $\mathbf{k}_{ij}^{(l)}$ is a column vector containing the stacked values of the function $2\tilde{c}_{ij}^{(l)}/(\sigma_w\sqrt{\pi})\Re\{\tilde{g}_{ij,p}^{(l)}G(f,\tilde{m}_{ij,p}^{(l)},(\sigma_{ij,3,p}^{(l)})^2)\exp(j(\tilde{\theta}_{ij,p}^{(l)}-\tilde{\vartheta}_{F_{ij}}^{(l)}))\}$ for increasing values of q. The expression of the roots x_k, $k=1,2,3$, of (11) are given by $x_k=-(b_1+\zeta^k A_1+B_1/(\zeta^k A_1))/(3a_1)$, where $a_1=2||\mathbf{G}||_2^2$, $b_1=3\mathbf{G}^T\mathbf{k}_{ij}^{(l)}$, $B_1=b_1^2-3a_1[||\mathbf{k}_{ij}^{(l)}||_2^2-2(\hat{\mathbf{S}}_{ij,p}-(\tilde{c}_{ij}^{(l+1)})^2\mathbf{y}_{ij}^{(l)})^T\mathbf{G}]$, and $A_1=[(C_1\pm\sqrt{-27\Delta_1 a_1^2})/2]^{1/3}$, in which $C_1=2b_1^3-9a_1b_1[||\mathbf{k}_{ij}^{(l)}||_2^2-2(\hat{\mathbf{S}}_{ij,p}-(\tilde{c}_{ij}^{(l+1)})^2\mathbf{y}_{ij}^{(l)})^T\mathbf{G}]-27a_1^2(\mathbf{k}_{ij}^{(l)})^T(\hat{\mathbf{S}}_{ij,p}-(\tilde{c}_{ij}^{(l+1)})^2\mathbf{y}_{ij}^{(l)})$ and the discriminant Δ_1 is given in (12) [see the top of the next page]. The new estimate $\tilde{C}_{F_{ij}}^{(l+1)}$ is the non-negative real-valued root x_k of (11) that minimizes the right-hand-side of (8). By substituting the new estimates $\tilde{c}_{ij}^{(l+1)}$ and $\tilde{C}_{F_{ij}}^{(l+1)}$ in (8), the problem in (8) reduces to the optimization problem described in (13) [see the top of the next page]. Then, the new estimates of $\tilde{k}_{ij,p}^{(l+1)}$, $\tilde{\theta}_{ij,0}^{(l+1)}$, $\tilde{\vartheta}_{F_{ij}}^{(l+1)}$, $\tilde{v}_p^{(l+1)}$, $\tilde{\beta}_{v,p}^{(l+1)}$, $\tilde{\alpha}_{v,p}^{(l+1)}$, $(\tilde{\beta}_{j,p}^{T})^{(l+1)}$, $(\tilde{\alpha}_{j,p}^{T})^{(l+1)}$, $(\tilde{\beta}_{i,p}^{R})^{(l+1)}$, and $(\tilde{\alpha}_{i,p}^{R})^{(l+1)}$ are numerically computed according to (13).

The iterative procedure in (6)−(13) is performed at each time instant t_p and proceeds as long as the objective function $E(\mathcal{P}_p)$ is higher than the predefined error ε.

IV. Numerical Results

Numerical results are presented in this section to validate the proposed iterative estimation algorithm. To this end, we compare the exact TV Doppler frequencies and speed with the corresponding estimated quantities. As explained in Section I, this task cannot be achieved with measurements data, for which the exact TV velocity of the person, i.e., TV speed, TV VAOM, and TV HAOM, is unknown. Therefore, we will consider a generated waveform sample of the complex channel gains $\mu_{ij}(t)$ and then compute the corresponding spectrograms by following the procedure reported in [26]. The spectrograms of the complex channel gain $\mu_{ij}(t)$ will play the role of the measured spectrograms $\hat{S}_{ij}(f,t)$ for $i,j=1,2,3$. The advantage of using a generated waveforms $\mu_{ij}(t)$ instead of real-valued channels is that the model parameters, including the velocity parameters, are known. This allows to fairly evaluate the accuracy of the proposed estimation algorithm by comparing the true velocity parameters to the estimated velocity parameters.

For the performance analysis, we consider a room of length A, width B, and height H equal to 14 m, 7 m, and 2.4 m, respectively. The locations of the transmit and receive antennas A_1^T, A_2^T, A_3^T, A_1^R, A_2^R, and A_3^R were $(5,2.5,2.25)$, $(-5,2.5,2.25)$, $(5,-2.5,-2.25)$, $(5,2.5,2.25)$, $(5,2.5,-2.25)$, and $(-5,-2.5,2.25)$, respectively. Here, we considered a single moving person. The trajectory of the person is assumed to be linear, while that of the moving scatterer S^M, representing the person's head, is modeled as [27] $z(t)=h_{\text{step}}\cos(2\pi f_{\text{step}}t)+h_{\text{head}}$, where the step height h_{step} is 2,7 cm and the height of the person h_{head} is 1.7 m. The walking frequency f_{step} is equivalent to the horizontal speed, which was set to 0.8 m/s, assuming a step length of

$$\Delta_1 = -108\,||\mathbf{G}||_2^2\,\mathbf{G}^T\mathbf{k}_{ij}^{(l)}\left[\left|\left|\mathbf{k}_{ij}^{(l)}\right|\right|^2 - 2\left(\hat{\mathbf{S}}_{ij,p} - \left(\tilde{c}_{ij}^{(l+1)}\right)^2\mathbf{y}_{ij}^{(l)}\right)^T\mathbf{G}\right]\left(\mathbf{k}_{ij}^{(l)}\right)^T\left(\hat{\mathbf{S}}_{ij,p} - \left(\tilde{c}_{ij}^{(l+1)}\right)^2\mathbf{y}_{ij}^{(l)}\right)$$
$$+108\left(\mathbf{G}^T\mathbf{k}_{ij}^{(l)}\right)^3\left(\mathbf{k}_{ij}^{(l)}\right)^T\left(\hat{\mathbf{S}}_{ij,p} - \left(\tilde{c}_{ij}^{(l+1)}\right)^2\mathbf{y}_{ij}^{(l)}\right) + 9\left(\mathbf{G}^T\mathbf{k}_{ij}^{(l)}\left[\left|\left|\mathbf{k}_{ij}^{(l)}\right|\right|^2 - 2\left(\hat{\mathbf{S}}_{ij,p} - \left(\tilde{c}_{ij}^{(l+1)}\right)^2\mathbf{y}_{ij}^{(l)}\right)^T\mathbf{G}\right]\right)^2$$
$$-8\,||\mathbf{G}||_2^2\left[\left|\left|\mathbf{k}_{ij}^{(l)}\right|\right|^2 - 2\left(\hat{\mathbf{S}}_{ij,p} - \left(\tilde{c}_{ij}^{(l+1)}\right)^2\mathbf{y}_{ij}^{(l)}\right)^T\mathbf{G}\right]^3 - 108\,||\mathbf{G}||_2^4\left(\left(\mathbf{k}_{ij}^{(l)}\right)^T\left(\hat{\mathbf{S}}_{ij,p} - \left(\tilde{c}_{ij}^{(l+1)}\right)^2\mathbf{y}_{ij}^{(l)}\right)\right)^2. \quad (12)$$

$$\left(\tilde{k}_{ij,p}^{(l+1)}, \tilde{\theta}_{ij,0}, \tilde{\vartheta}_{F_{ij}}^{(l+1)}, \tilde{v}_p^{(l+1)}, \tilde{\beta}_{v,p}^{(l+1)}, \tilde{\alpha}_{v,p}^{(l+1)}, \left(\tilde{\beta}_{j,p}^T\right)^{(l+1)}, \left(\tilde{\alpha}_{j,p}^T\right)^{(l+1)}, \left(\tilde{\beta}_{i,p}^R\right)^{(l+1)}, \left(\tilde{\alpha}_{i,p}^R\right)^{(l+1)}\right) = \underset{\mathcal{P}_p\setminus\{\tilde{c}_{ij},\tilde{C}_{F_{ij}}\}}{\operatorname{argmin}}\left\{\sum_{i,j=1}^{3}\left\|\hat{\mathbf{S}}_{ij,p} - \left(\tilde{c}_{ij}^{(l+1)}\right)^2\right.\right.$$
$$\left.\left. G\left(f_q, \tilde{f}_{ij,p}, \tilde{\sigma}_{ij,1,p}^2\right) - \mathbf{G}\left(\tilde{C}_{F_{ij}}^{(l+1)}\right)^2 - \frac{2\tilde{c}_{ij}^{(l+1)}\tilde{C}_{F_{ij}}^{(l+1)}}{\sigma_w\sqrt{\pi}}\Re\left\{\tilde{g}_{ij,p}G\left(f, \tilde{m}_{ij,p}, \sigma_{ij,3,p}^2\right)\exp\left(j\left(\tilde{\theta}_{ij,p} - \tilde{\vartheta}_{F_{ij}}\right)\right)\right\}\right\|_2^2\right\} \quad (13)$$

30 cm. The observation time interval is taken to be [0,5s]. Our considered fall scenario can be divided into three phases. First, the person starts walking with a constant speed for 2.5 s, which corresponds to a distance of 2 m. Then, the person starts to fall forward until his/her head reaches the floor. This phase lasts 1 s. Finally, the person's body reaches the floor and stops moving for the rest of the observation time. The TV HAOM and TV VAOM have been computed based on the initial and final locations of S^M. The number of fixed scatterers has been set to $M_{ij} = 7$ with $\sum_{m_{ij}=1}^{M_{ij}} c_{m_{ij}}^2 = 1$. Also, the carrier frequency f_0 has been set to 5.9 GHz. The parameter σ_w^2 has been chosen to be $\sigma_w^2 = \min(1/\sqrt{2\pi|k_{ij}(t_l)|})$. In the following, the error level ε is 0.01.

Figs. 3 and 4 depicts the TV speed $v(t)$ and TV VAOM $\beta_v(t)$ of the moving person S^M with the corresponding estimated values, respectively. A good match can be observed between both quantities which confirms the validity and accuracy of the proposed velocity estimation algorithm. Together with the TV speed, TV VAOM, and TV HAOM, the iterative procedure described in Section III, estimates the gains, initial phase of the channel, VAOD, HAOD, VAOA, and HAOA, which in turn allows us to compute the corresponding estimated TV Doppler frequencies $f_{ij}(t)$ and TV Doppler shifts $B_{\mu_{ij}}^{(1)}(t)$ according to (2) and [26, Eq. (41)], respectively. In Fig. 5, we present the TV Doppler frequencies $f_{ij}(t)$ with the corresponding estimated quantities. For brevity, only results for the TV Doppler frequencies $f_{11}(t)$ and $f_{31}(t)$ and the TV Doppler shifts $B_{\mu_{11}}^{(1)}(t)$ and $B_{\mu_{31}}^{(1)}(t)$ are presented. It should be mentioned that similar results are obtained for the all TV Doppler frequencies and TV mean Doppler shifts.

Comparison with other methods: For the performance assessment of the proposed algorithm, it is important to compare the results obtained with the estimation algorithm with those obtained by applying other RF-based estimation techniques. To the best of the authors' knowledge, the only RF-based method that can be considered for this purpose is that employed in the WiGait device [23]. Unfortunately, no details regarding the employed algorithm are available in the literature. In addition, speed estimation methods developed in the context of mobile-radio communications cannot be considered due to their limited applicability to WSS channels [1], [10]. Hence, a comparison with other speed estimators cannot be presented.

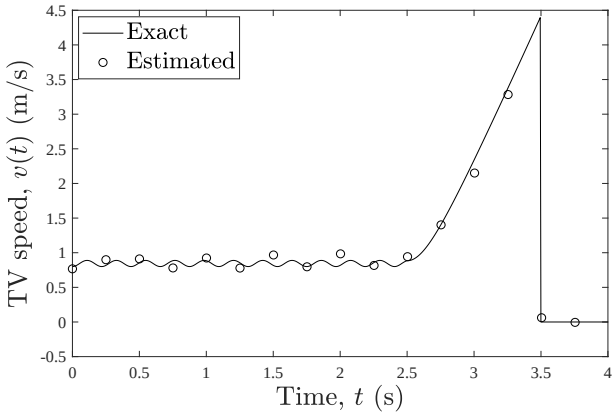

Fig. 3. TV speed $v(t)$ of the moving scatterer (person) S^M.

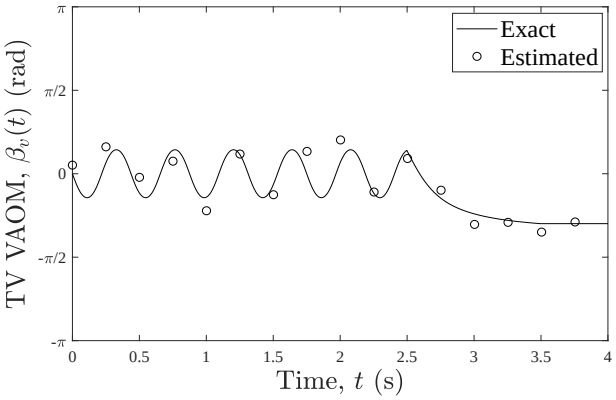

Fig. 4. TV VAOM $\beta_v(t)$ of the moving scatterer (person) S^M.

V. Conclusion

This paper proposes a new iterative procedure to estimate the velocity of a single moving person in three-dimensional indoor environments equipped with a distributed 3×3 MIMO system using radio-frequency techniques. This method esti-

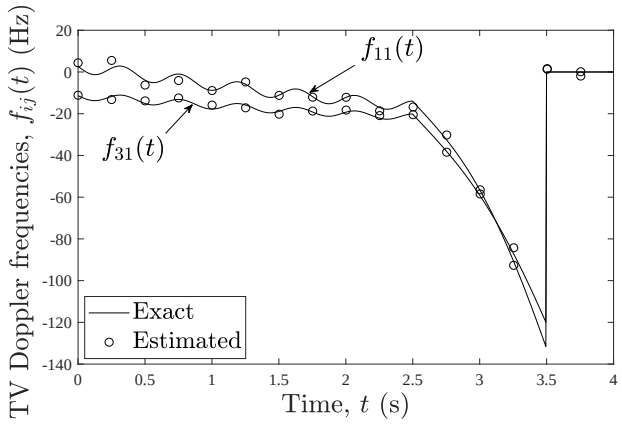

Fig. 5. TV Doppler frequencies $f_{ij}(t)$.

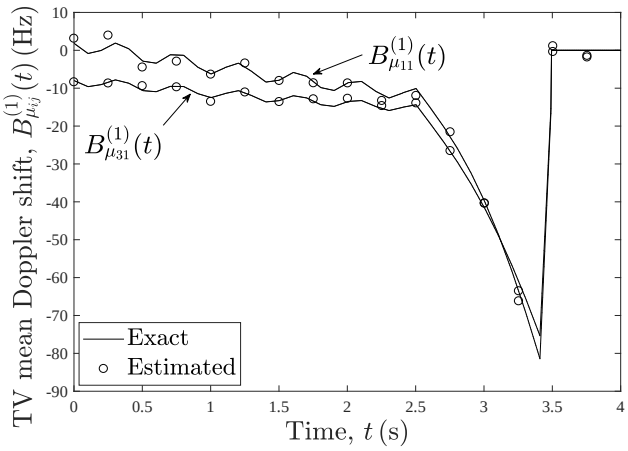

Fig. 6. TV mean Doppler Shift $B^{(1)}_{\mu_{ij}}(t)$.

mates the TV velocity, i.e., TV speed, TV VAOM, and TV HAOM, by fitting the spectrogram of the channel model to the spectrogram computed from the received radio signals. The good match between the exact TV speed, TV VAOM, TV Doppler frequencies, and TV mean Doppler shift and the corresponding estimated quantities confirms the validity of the proposed estimation technique.

ACKNOWLEDGEMENT

This work was supported by the WiCare Project funded by the Research Council of Norway under grant number 261895/F20.

REFERENCES

[1] G. L. Stüber, *Principles of Mobile Radio Communications*, Kluwer, MA, USA, 2nd edition, 2000.

[2] M. D. Austin and G. L. Stüber, "Velocity adaptive handoff algorithms for microcellular systems," *IEEE Trans. Veh. Technol.*, vol. 43, no. 3, pp. 549–561, 1994.

[3] Y. Zhuang et al., "An iterative Doppler shift estimation in vehicular communication systems," *Procedia Engineering*, vol. 29, pp. 4129–4134, 2012.

[4] J. M. Holtzman and A. Sampath, "Adaptive averaging methodology for handoffs in cellular systems," *IEEE Trans. Veh. Technol.*, vol. 44, no. 1, pp. 59–66, Feb. 1995.

[5] K. D. Anim-Appiah, "On generalized covariance-based velocity estimation," *IEEE Trans. Veh. Technol.*, vol. 48, no. 5, pp. 1546–1557, Sep. 1999.

[6] C. Tepedelenlioğlu, A. Abdi, G. B. Giannakis, and M. Kaveh, "Estimation of Doppler spread and signal strength in mobile communications with applications to handoff and adaptive transmission," *Wireless Commun. and Mobile Comput.*, vol. 1, no. 2, pp. 221–242, 2001.

[7] L. Krasny, H. Arslan, D. Koilpillai, and S. Chennakeshu, "Doppler spread estimation in mobile radio systems," *IEEE Commun. Letters*, vol. 5, no. 5, pp. 197–199, May 2001.

[8] G. Lindgren, "Spectral moment estimation by means of level crossings," *Biometrika*, vol. 61, no. 2, pp. 401–418, Dec. 1974.

[9] A. Abdi and S. Nader-Esfahani, "Expected number of maxima in the envelope of a spherically invariant random process," *IEEE Trans. Inf. Theory*, vol. 49, no. 5, pp. 1369–1375, May 2003.

[10] H. Zhang and A. Abdi, "Nonparametric mobile speed estimation in fading channels: Performance analysis and experimental results," *IEEE Trans. Wireless Commun.*, vol. 8, no. 4, pp. 1683–1692, Apr. 2009.

[11] M. Ermes, J. Pärkkä, J. Mäntyjärvi, and I. Korhonen, "Detection of daily activities and sports with wearable sensors in controlled and uncontrolled conditions," *IEEE Trans. Inf. Technol. Biomed.*, vol. 12, no. 1, pp. 20–26, Jan. 2008.

[12] C. Strohrmann, H. Harms, C. Kappeler-Setz, and G. Tröster, "Monitoring kinematic changes with fatigue in running using body-worn sensors," *IEEE Trans. Inf. Technol. Biomed.*, vol. 16, no. 5, pp. 983–990, Sept. 2012.

[13] B. Mariani, M. C. Jiménez, F. J. G. Vingerhoets, and K. Aminian, "On-shoe wearable sensors for gait and turning assessment of patients with Parkinson's disease," *IEEE Trans. Biomed. Eng.*, vol. 60, no. 1, pp. 155–158, Jan. 2013.

[14] E. E. Stone and M. Skubic, "Evaluation of an inexpensive depth camera for passive in-home fall risk assessment," in *5th Int. Conf. on Pervasive Computing Technol. for Healthcare (PervasiveHealth'11),*, 2011, pp. 71–77.

[15] C. Zhang and Y. Tian, "RGB-D camera-based daily living activity recognition," *J. of Comput. Vis. Image Process.*, vol. 2, no. 4, pp. 12, 2012.

[16] H. Sakaino, "Video-based tracking, learning, and recognition method for multiple moving objects," *IEEE Trans. Circuits Sys. for Video Technol.*, vol. 23, no. 10, pp. 1661–1674, Oct. 2013.

[17] P. Leusmann, C. Möllering, L. Klack, K. Kasugai, M. Ziefle, and B. Rumpe, "Your floor knows where you are: Sensing and acquisition of movement data," in *12th Int. Conf. on Mobile Data Management (MDM'11)*, 2011, vol. 2, pp. 61–66.

[18] S. C. Mukhopadhyay, "Wearable sensors for human activity monitoring: A review," *IEEE Sens. J.*, vol. 15, no. 3, pp. 1321–1330, Mar. 2015.

[19] J. Bae and M. Tomizuka, "A tele-monitoring system for gait rehabilitation with an inertial measurement unit and a shoe-type ground reaction force sensor," *Mechatronics*, vol. 23, no. 6, pp. 646–651, Sep. 2013.

[20] "Run3D," Ltd. Available: http://www.run3d.co.uk/healthcare-professionals/about-our-run3d-system.

[21] "Emerald (2015) [Online]," Available: http://www.emeraldforhome.com/.

[22] Z. Yang, P. H. Pathak, Y. Zeng, X. Liran, and P. Mohapatra, "Monitoring vital signs using millimeter wave," in *17th ACM Int. Symp. on Mobile Ad Hoc Networking and Computing (ACM'16)*, 2016, pp. 211–220.

[23] C.-Y. Hsu, Y. Liu, Z. Kabelac, R. Hristov, D. Katabi, and C. Liu, "Extracting gait velocity and stride length from surrounding radio signals," in *Proc. of the ACM Conf. on Human Factors in Computing Systems (CHI'17)*, Denver, USA, May 2017, pp. 2116–2126.

[24] M. G. Amin, Y. D. Zhang, F. Ahmad, and K. C. D. Ho, "Radar signal processing for elderly fall detection: The future for in-home monitoring," *IEEE Signal Process. Mag.*, vol. 33, no. 2, pp. 71–80, Mar. 2016.

[25] Z. Jiang et al., "Communicating is crowdsourcing: Wi-Fi indoor localization with CSI-based speed estimation," *J. of Computer Science and Technol.*, vol. 29, no. 4, pp. 589–604, Jul. 2014.

[26] A. Abdelgawwad and M. Pätzold, "A framework for activity monitoring and fall detection based on the characteristics of indoor channels," in *IEEE 87th Veh. Technol. Conf. (VTC'18-Spring)*, Porto, Portugal, Jun. 2018, pp. 1–7.

[27] S.-U. Jung and Mark S. Nixon, "Estimation of 3D head region using gait motion for surveillance video," in *4th Int. Conf. on Imaging for Crime Detection and Prevention (ICDP'11)*, London, UK, Nov. 2011, pp. 1–6.